Biosensors and Bioelectronics 237 (2023) 115451

Contents lists available at ScienceDirect

Biosensors and Bioelectronics

journal homepage: www.elsevier.com/locate/bios

Multistage microfluidic cell sorting method and chip based on size and stiffness

Gaolin Li [a,b], Yuan Ji [a], Yihui Wu [a,*], Yongshun Liu [a], Huan Li [a,**], Yimeng Wang [a,b], Mingbo Chi [a], Hongyan Sun [c], Hongquan Zhu [c]

[a] Changchun Institute of Optics, Fine Mechanics and Physics (CIOMP), Chinese Academy of Sciences, Changchun, China
[b] University of Chinese Academy of Sciences, Beijing, China
[c] Department of Clinical Laboratory, The Second Hospital of Jilin University, Changchun, China

ARTICLE INFO

Keywords:
Microfluidic chip
Deterministic lateral displacement
Cone channel chip
Cell sorting

ABSTRACT

High performance sorting of circulating tumor cells (CTCs) from peripheral blood is key to liquid biopsies. Size-based deterministic lateral displacement (DLD) technique is widely used in cell sorting. But conventional microcolumns have poor fluid regulation ability, which limits the sorting performance of DLD. When the size difference between CTCs and leukocytes is small (e.g., less than 3 μm), not only DLD, many size-based separation techniques fail due to low specificity. CTCs have been confirmed to be softer than leukocytes, which could serve as a basis for sorting. In this study, we presented a multistage microfluidic CTCs sorting method, first sorting CTCs using a size-based two-array DLD chip, then purifying CTCs mixed by leukocytes using a stiffness-based cone channel chip, and finally identifying cell types using Raman techniques. The entire CTCs sorting and analysis process was label free, highly pure, high-throughput and efficient. The two-array DLD chip employed a droplet-shaped microcolumn (DMC) developed by optimization design rather than empirical design. Attributed to the excellent fluid regulation capability of DMC, the CTCs sorter system developed by parallelizing four DMC two-array DLD chips was able to process a sample of 2.5 mL per minute with a recovery efficiency of 96.30 ± 2.10% and a purity of 98.25 ± 2.48%. To isolate CTCs mixed dimensionally by leukocytes, a cone channel sorting method and chip were developed based on solid and hydrodynamic coupled analysis. The cone channel chip allowed CTCs to pass through the channel and entrap leukocytes, improving the purity of CTCs mixed by leukocytes by 1.8-fold.

1. Introduction

Sorting methods with high purity, efficiency, and cell viability become key to the clinical application of circulating tumor cells (CTCs) (Henry et al., 2016; Vaidyanathan et al., 2019). Label-free separation not only maintains activity and integrity but is more easily compatible with downstream analysis such as NGS (Thompson et al., 2014; Yeo et al., 2016). Size-based deterministic lateral displacement (DLD) technique is being widely used to separate various particles such as blood cells (Zeming et al., 2016), CTCs (Jiang et al., 2017; Au et al., 2017), and bacteria (Beech et al., 2018; Pariset et al., 2018) due to the advantages of label-free and high throughput (Huang et al., 2004; Beech et al., 2009). In a DLD field, the flow within the microcolumn gap was divided evenly by the period number of the microcolumn array, and the flow beam nearest the tip of the microcolumn was called the first flow beam, the width of which was approximately the critical radius of the microcolumn array (Inglis et al., 2006). Particles larger than the critical diameter move in a migration mode along the offset direction of microcolumns, and particles smaller move in a Zigzag mode along a straight line. Lower critical diameter, higher resolution, less clogging, and higher throughput are promising developments for DLD (Hochstetter et al., 2020).

The conventional microcolumn shapes have poor fluid regulation ability, which limits the sorting performance of DLD. Microcolumns with lower critical diameter D_c not only allow easy sorting of small-sized particles, but also have larger gap and throughput, shorter arrays length, and less clogging (Loutherback et al., 2010). According to Eq. (1) obtained by Davis (2008) and Zhang et al. (2015), critical diameter D_c is

* Corresponding author.
** Corresponding author.
E-mail addresses: yihuiwu@ciomp.ac.cn (Y. Wu), lihuan@ciomp.ac.cn (H. Li).

https://doi.org/10.1016/j.bios.2023.115451
Received 17 March 2023; Received in revised form 13 May 2023; Accepted 5 June 2023
Available online 12 June 2023

positively proportional to the gap G and negatively correlated with the period N, and can be estimated from the first flow beam width d_0. So it is difficult to design smaller D_c, larger G (i.e., higher throughput and less clogging), and smaller N (i.e., shorter array length and higher yield) simultaneously. Some new microcolumn shapes such as winged (Al-Fandi et al., 2011), triangular (Loutherback et al., 2010), asymmetric (Au et al., 2017), I-shaped (Zeming et al., 2013), and inverted heart-shaped (Chen et al., 2022) were developed to improve the sorting performance, but different shapes have slightly different interaction mechanisms with fluids, so it is difficult to find the ideal microcolumn shape by empirical design.

$$D_c = 1.4G\left(\frac{1}{N}\right)^{0.48} \approx 2d_0 \tag{1}$$

Due to the low specificity, size-based separation techniques such as DLD, microfiltration, and inertial microfluidics fail when CTCs and leukocytes are close in size, which results in mixing leukocytes to decrease CTCs purity and cover up cancer information (Qian et al., 2015; Wills and Mead, 2015) or losing small-sized CTCs. The size of CTCs ranges from 4 ~ 30 μm (Allard et al., 2004) and most leukocytes are around 10 μm (Cormack, 2001; Seifter et al., 2005; Loiko et al., 2007), so actually sizes overlap significantly. CTCs of breast cancer patients are generally larger or similar to leukocytes (Hyun et al., 2013), and CTCs smaller than leukocytes have been found (Marrinucci et al., 2010). The high heterogeneity and complexity make it difficult to rely on single size differences to achieve complete CTCs sorting. Hybrid sorting methods were developed based on multiple attributes to further isolate CTCs mixed dimensionally by leukocytes, such as using fluorescence-activated acoustics to sort cells pre-enriched by inertial focusing (Zhou et al., 2019), using magnetophoretic technology to sort CTCs after DLD and inertial focusing processing (Karabacak et al., 2014), but markers are costly and affect cell activity (Hou et al., 2013), and false negative/-positive results may limit sort purity (Low and Wan Abas, 2015), and external force field increases the system complexity.

Stiffness is another property validated for classification. As shown in Table 1, cancer cells are softer compared to normal cells (Roca-Cusachs et al., 2006; Kuznetsova et al., 2007), so Young's modulus perhaps reflects the histological background and distinguish between non-metastatic and metastatic cells (Low and Wan Abas, 2015). A series of channels with diagonal ridges have been used for stiffness-based sorting of epithelial cancer cells (Wang et al., 2013), leukemia cells (Islam et al., 2020), and live and dead cells (Islam et al., 2017), but repeatedly squeezing cells may damage cells. Leukemia cells and natural killer cells with different compressibility were separated in the divergent channel according to the difference of acoustic radiation force caused by compressibility (Xue et al., 2023). However, this required a complex tilted surface acoustic wave device.

Table 1
Young's modulus of cancer cells and benign cells.

cell types	Young's modulus (kPa)	literature
melanoma cells	0.88±0.13	Celik et al. (2015)
leukocytes	1.96±0.52	
human ovarian cancer HEY cells	0.88±0.53	Xu et al. (2012)
human ovarian cancer HEY A8 cells	0.49±0.22	
nonmalignant ovarian epithelial cells	2.47±2.05	
highly metastatic human prostate PC3 cells	0.13	Chen et al. (2013)
nonmalignant human prostate BPH-1 cells	3.7	
metastatic breast cancer cells	0.53±1.10	Cross et al. (2007)
corresponding benign mesothelial cells	1.97±0.07	
non-small cell lung cancer cells	0.52±0.12	Cross et al. (2007)
corresponding benign mesothelial cells	2.05±0.87	

In this paper, we first newly developed a droplet-shaped microcolumn (DMC) to improve the sorting performance of DLD. The DMC was obtained by optimizing the flow distribution within the microcolumn gap with the goal of reducing the first flow beam width. Due to a 21.25 ± 1.91% reduction in critical size, the throughput of DMC increased by 28% compared to circular microcolumn (CMC). Due to fewer tips and lower flow separation, DMC has a shorter array length, smoother flow guidance, and more cell friendliness compared to triangular microcolumn (TMC). The CTCs sorter system was then developed by parallelizing four DMC two-array DLD chips with critical sizes of 8 μm and 13 μm, and this system was able to process a sample of 2.5 mL per minute with a recovery efficiency of 96.30 ± 2.1% and a purity of 98.25 ± 2.48%, which surpassed most label free technologies. To isolate CTCs mixed dimensionally by leukocytes, we also developed a stiffness-based cone channel sorting method through solid and hydrodynamic coupling analysis among cells, channel boundaries, and fluids. The cone channel chip improved the purity of CTCs mixed by leukocytes by 1.8-fold. Rama technology finally successfully identified cancer cells and leukocytes. Based on the novel DMC and chips, the multistage cell sorting and analysis process was label-free, highly pure, high-throughput and efficient, and capable of handling real clinical samples.

2. Multistage separation scheme

According to the size of CTCs, we classified the cells into three sizes: large diameter ($>13\mu m$), medium diameter (8 ~ 13 μm), and small diameter ($<8\mu m$). A small number of CTCs are in the medium diameter, and they are not easily isolated by size-based microfluidic techniques due to the interference of leukocytes. Within the DMC two-array DLD chip (Fig. 1), small-diameter cells maintained Zigzag mode motion at the bottom of the chip throughout. Medium - and large-diameter cells moved to the middle of the chip in a migratory mode in the first array and separated in the second array. The three sizes of cells were sorted out from the bottom outlet, the middle outlet and the top outlet, respectively. The medium-diameter CTCs and leukocytes were then purified through cone channel chips. Stiffer leukocytes were entrapped while softer CTCs passed through the channel. The cell types were finally identified using a Raman microspectrophotometer, which is compatible with label free sorting chips.

3. Optimizing the DLD flow field to obtain the DMC

3.1. Optimization method

A parametric CMC array fitted by Bezier curves was constructed using COMSOL multiphysics (Fig. 2a). Control point b was set at the position of the first flow beam on observation line $\overline{ac}$ shown in Fig. 2b. Since the flow within the longitudinal gap is uniformly distributed by period N (Huang et al., 2004), the higher the flow through the first flow beam $\overline{ab}$, the smaller first flow beam width d_0 and critical diameter D_c. The optimization goal Obj (Eq. (2)) thus was that the ratio of flow within the first flow beam to that of the gap was highest. We kept the period N to 10 and set a diameter of 30 ~ 80 μm and a gap of 15 ~ 35 μm. The abscissa and ordinate of the fitting points were added a scaling coefficient (k_i, m_i) with a value range of [0.6, 2] and an initial value of 1. Since the first flow beam is mainly regulated by the morphology of the microcolumn top, fitting points P_1, P_7, and P_{10} were fixed to decrease computational cost. Since the physical characteristics of the working fluid phosphate buffer (PBS) and water are close at room temperature, the working fluid was set to incompressible water and was described by Navier-Stokes and continuity equations. The inlet flow was 0.05 m/s to maintain a stable laminar flow. The top and bottom of the model were kept equal in velocity and pressure to circumvent the perturbation. The constraints were given as Eq. (3) and this derivative agnostic nonlinear structure shape optimization problem was solved by the

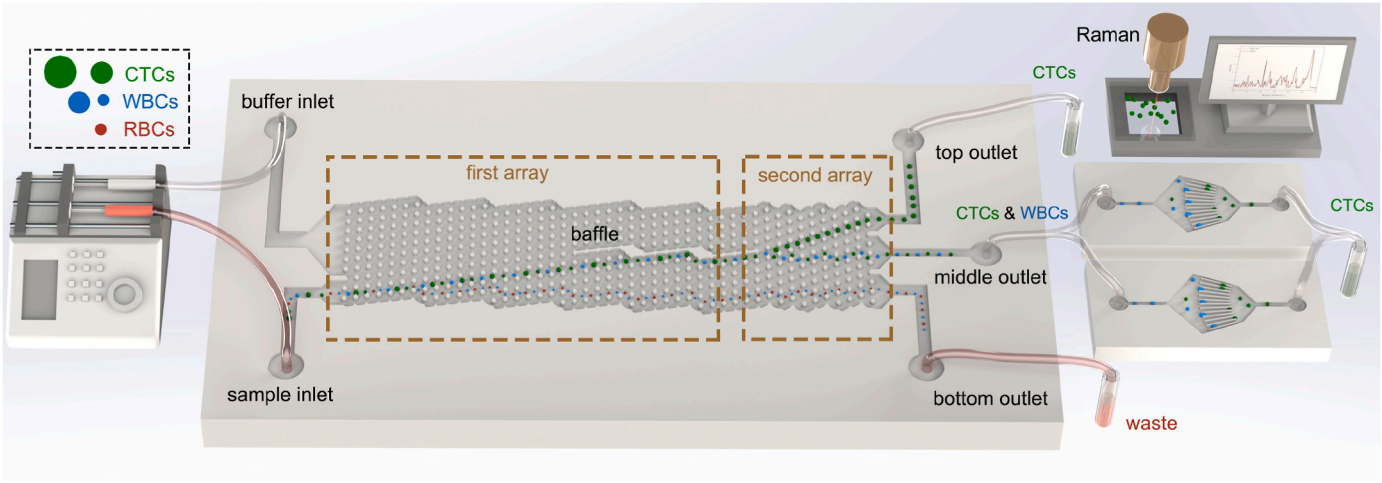

Fig. 1. Schematic illustration of the multistage microfluidic sorting system based on size and stiffness. The DMC had a height of 50 μm and a gap of 32 μm. The DMC two-array DLD chip had a total period of 32. The critical sizes of the first and second arrays were 8 μm and 13 μm, and the critical size accuracies were 90% and 94.85%, respectively (see SI for details). Each cone channel chip included 104 single cone channels with an inlet width of 13 μm, an outlet width of 8 μm, a taper of 1 : 20, and a channel depth of 25 μm.

comparative-based Nelder-Mead method.

3.2. Optimization results

The CMC array turned into the DMC array after optimization (Fig. 2c). The average DMC (Fig. 2d) was obtained by averaging the scaling coefficients. See SI for DMC details and see video S1 for optimization process. DMC combines the advantages of the short array length of CMC and the low critical size of TMC, which can be considered as a CMC with a top protrusion forming a tip, or a TMC with a bottom edge extending outward to form an arc (Fig. 2e). DMC accelerates the first flow beam through the longitudinal gap and impedes it from crossing the transverse gap, which is not achievable by CMC and TMC.

3.3. Fluid regulation capability analysis

Compared to CMC, the area on both sides of the tip of DMC and TMC increased the fluid motion space, which decreased the pressure nearby and increased the flow rate (Fig. 3a). Due to the equal flow of each flow beam, the first flow beam reduces its width and can only carry smaller-sized particles, which reduces the critical size. The critical diameter of the DMC calculated by Eq. (4) decreased by 21.25 ± 1.91% compared with the CMC, which was consistent with the simulation (Fig. 3b). When sorting particles of the same size, the gap of DMC needs to be set to 128% of the gap of CMC, thus increasing the throughput by 28%. See SI for details and see videos S2 ~S3 for particle trajectories.

$$\begin{cases} N\int_0^{d_0} u(s)ds = \int_0^{G} u(s)ds \\ D_c \approx 2d_0 \end{cases} \tag{4}$$

The higher flow separation (Fig. 3c) within the transverse gap means that more fluid moves down, which is more likely to carry large-sized particles toward the bottom of the next microcolumn and improve critical size. Compared to TMC, the bottom edge of DMC expands significantly outward, occupying the front space of the fluid, which impedes the flow of the first flow beam and decreases the flow separation. The DMC had the lowest velocity within the transverse gap (Fig. 3d), and its flow separation (3.68%) was lower than that of the CMC (9.22%) and TMC (21.51%). Because the stream will return to initial position after one period, the actual period of DMC and TMC became 27 and 5 (theoretical value was 10), respectively. Therefore, when sorting particles of the same size, the period (i.e., array length) of DMC and TMC needs to be set to 37% and 200% of that of CMC, respectively. This is the reason why DLD chips with TMC need to set up very long arrays.

The smooth convex surface of the DMC and CMC guided the fluid smoother, while the flat side of the TMC and the drastically changing bottom tip resulted in fluid backflow as shown by the red circle of Fig. 3e, which increased particle trajectory uncertainty. The tip of TMC facing flow direction may cause cell damage.

4. A cone channel sorting method based on stiffness

As shown in Fig. 4a, in the X direction, a cell outside the channel and without rotation was only subjected to the shear-induced inertial lift force F_{IL} and the wall-induced lift force F_{WL}. After the cell was pushed into the channel by the hydrodynamic force F_h, the lift forces were replaced by the wall counterforce F_{cx}, which more easily compresses the cell, thus more clearly reflecting the difference in Young's modulus. In the Y direction, the numerical magnitude of wall counterforce F_{cy} and F_h determines whether the cell can move through the channel.

In a 3D solid mechanical contact simulation (see SI and video S7), a cell was first forced to pass through the cone channel to obtain counterforce F_{cy}, the value of which was obtained by integrating the counterforce of the fixed channel boundary along the Y direction. As the cell entered the channel and deformed, F_{cy} reached a maximum F_{cymax}. Since the adhesion and frictional were not set, F_{cy} was reduced to zero after the cell completely entered the end of the channel of equal width (Fig. 4b). Then in a 3D hydrodynamic simulation, the deformation and displacement of the cell when it was subjected to F_{cymax} was maintained. The fluid was injected from the inlet and the Navier-Stokes equation was solved, and integrated the pressure on the cell surface to obtain hydrodynamic force F_h, as shown in Fig. 4c.

The cell passes through the channel only if subjected to hydrodynamic force F_h sufficient to overcome the maximum counterforce F_{cymax}. Since F_h is usually controlled by adjusting the inlet flow Q in microfluidic devices, the critical inlet flow Q_c was obtained by equating the values of F_h and F_{cymax}, as shown in Fig. 4d. When Q is larger than Q_c, the cell will pass through the channel, otherwise it will be entrapped. For example, when the actual inlet flow Q is 0.46 μL/min, cells (10 μm $< D <$ 11 μm, $E >$ 1.5 kPa, e.g. leukocytes (Celik et al., 2015)) above the blue dotted line will be entrapped, whereas cells (10 μm $< D <$ 11 μm, $E <$ 1 kPa, e.g. human ovarian cancer HEY cells (Xu et al., 2012)) below this line will pass through the channel. Thus by controlling the flow rate, the cone channel enables separation of CTCs and leukocytes close in size. As

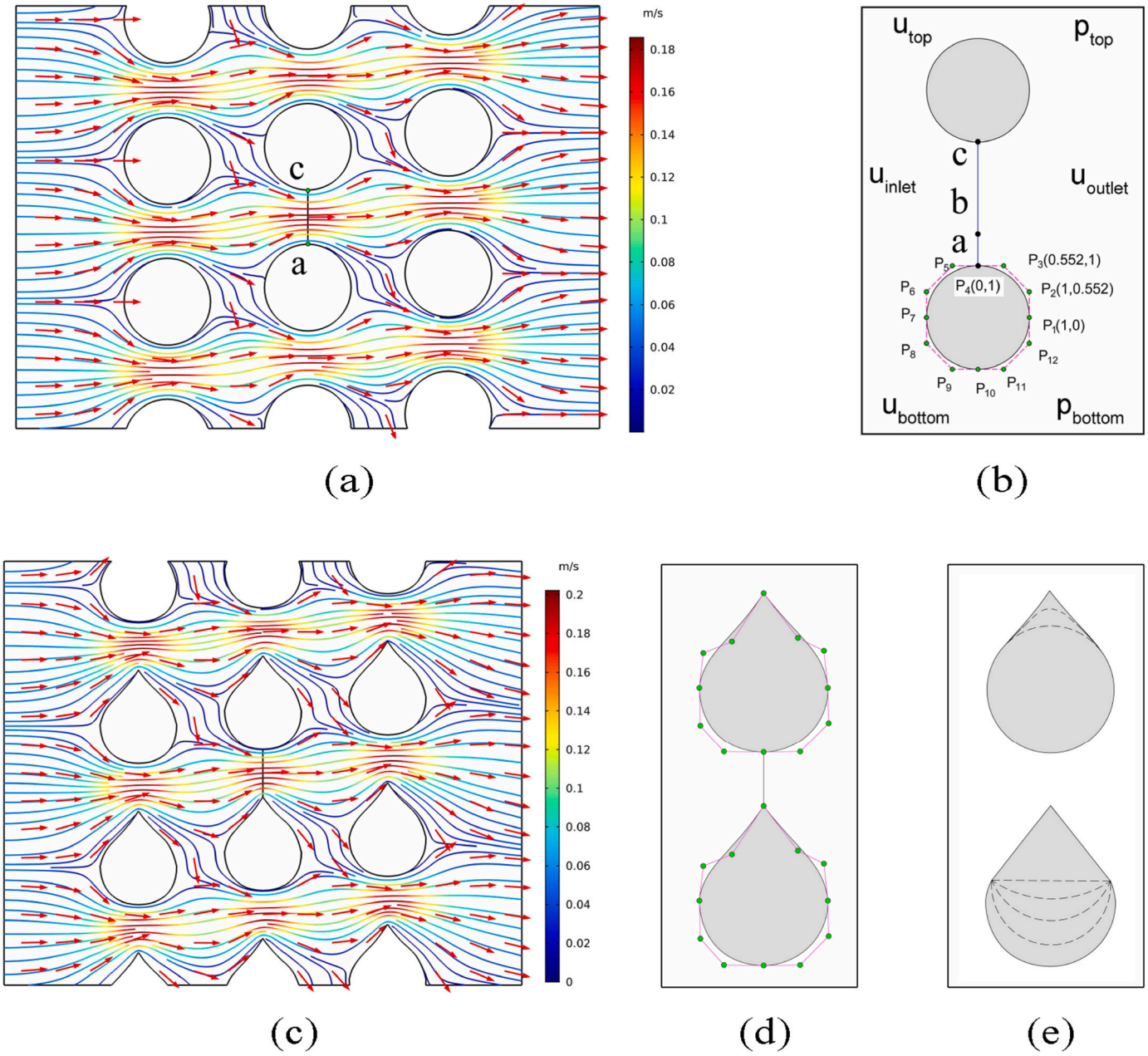

Fig. 2. (a) The optimization model was a CMC array of 3 × 3. (b) Settings of control point b, fitting points P_i and observation line $\overline{ac}$. (c) The DMC array after optimization. (d) The average DMC. (e) DMC can be seen as a deformation of TMC or CMC.

$$\max \quad Obj = \int_a^b u(s)ds \Big/ \int_a^c u(s)ds \tag{2}$$

$$s.t. \begin{cases} \rho(\boldsymbol{u}\cdot\nabla)\boldsymbol{u} = -\nabla p + \nabla\cdot\mu(\nabla\boldsymbol{u} + (\nabla\boldsymbol{u})^T) \\ \nabla\cdot\boldsymbol{u} = 0 \\ p_{top} - p_{bottom} = 0 \\ \boldsymbol{u}_{top} - \boldsymbol{u}_{bottom} = \boldsymbol{0} \\ 2Ny_b^3 - 3NGy_b^2 + G^3 = 0,\ 0 \leqslant y_b \leqslant G \ (\text{see SI}) \\ 0.6 \leqslant k_i, m_i \leqslant 2,\ i = 2, 3, \ldots, 11, 12 \ and \ i \neq 7, 10 \\ k_j, m_j = 1,\ j = 1, 7, 10 \end{cases} \tag{3}$$

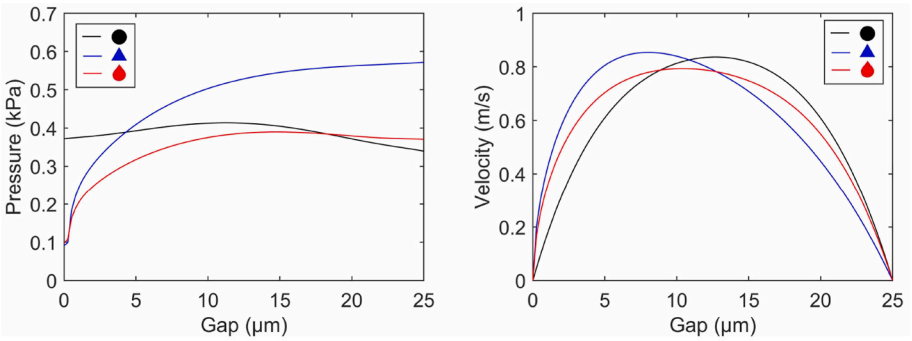

(a)

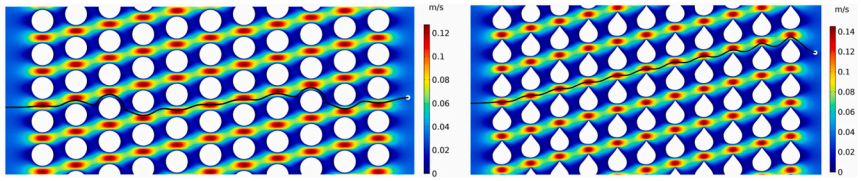

(b)

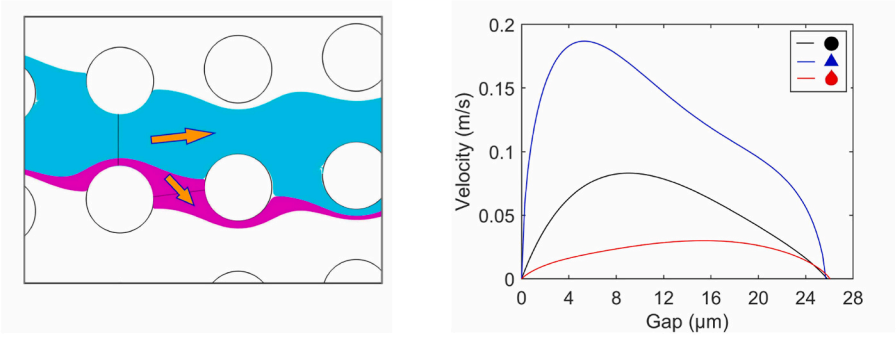

(c) (d)

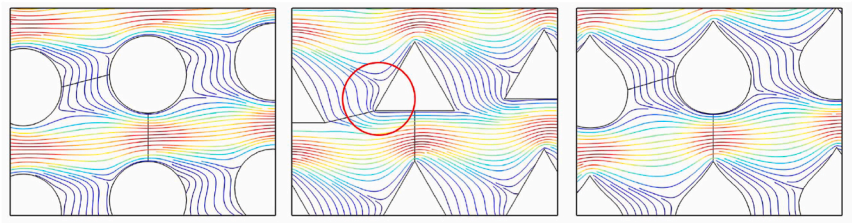

(e)

Fig. 3. (a) Pressure and velocity distribution within the longitudinal gap with the same flow rate. (b) Particles of the same size moved in Zigzag and migration modes within CMC and DMC arrays, respectively, indicating that the critical diameter of DMC was smaller than the CMC. (c) The fluid produces separation after passing through the longitudinal gap. (d) Velocity distribution within the transverse gap with the same longitudinal gap flow rate. (e) Flow field within CMC, TMC and DMC arrays.

shown in Fig. 5a, all medium-diameter DU145 cells would pass through the cone channel when the inlet flow rate of a single cone channel was 0.6526 μL/min, while leukocytes with a size larger than 10.37 μm would get trapped.

5. Experiments

5.1. Chip fabrication and cell culture methods

The preparation methods for microfluidic chips (Fig. 5b) and polyvinyl alcohol solution, as well as cell culture methods, are presented in the SI.

5.2. Measurement of Young's modulus

The Young's modulus of DU145 cells and leukocytes were measured to be 0.96 ± 0.21 kPa and 1.78 ± 0.27 kPa, respectively. See SI for details.

5.3. Experiment of the DMC two-array DLD chip

DU145 cells labeled using CFDA SE (Beyotime, CHN) were configured to a suspension with a concentration of 7.5×10^5/mL. After mixing 0.1 mL of DU145 cell suspension with 0.5 mL of healthy human whole blood, PBS was added to 10 mL as the separation sample solution. The number ratio of DU145 cells and blood cells in the sample was approximately $1 : 1 \times 10^5$. According to the ethical principles of the

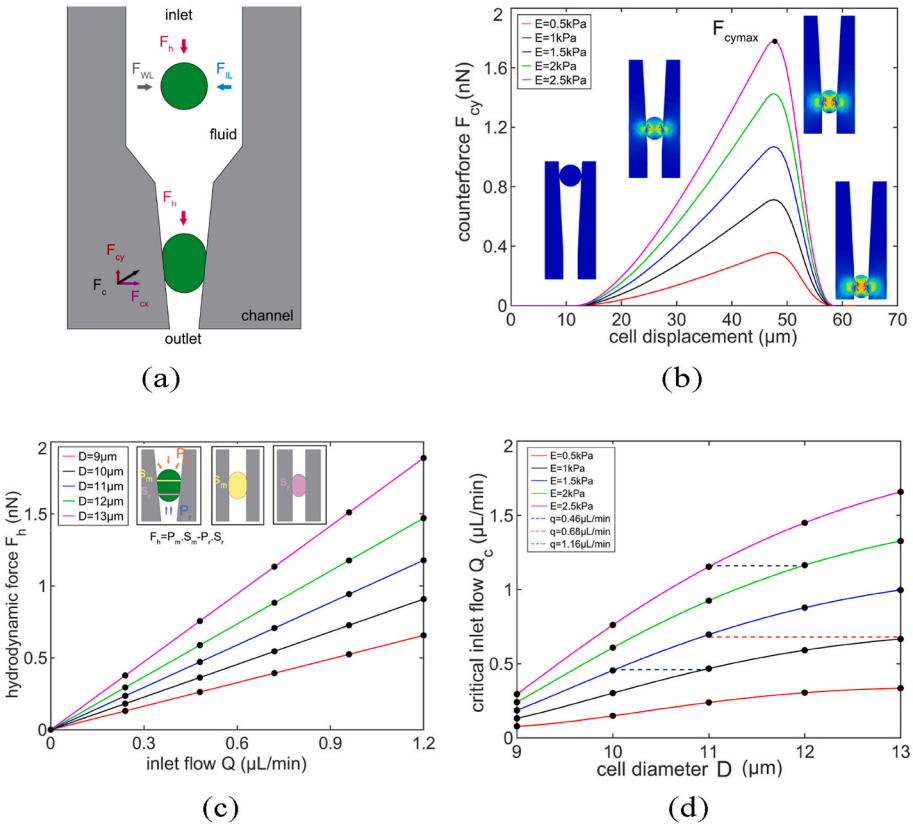

Fig. 4. (a) Forces on a cell outside and inside the cone channel. (b) Cells within the channel were subjected to counterforce F_{cy}. The cell had a diameter of 9 ~ 13 μm and Young's modulus of 0.5 ~ 2.5 kPa. The cone channel had an inlet width of 13 μm, an outlet width of 8 μm, a taper of 1 : 20 and a depth of 25 μm. The back end of the cone channel was set equal in width. (c) Hydrodynamic force F_h was obtained by integrating the pressure (P_m and P_r) and projection planes (yellow area S_m and red area S_r). Since the cell was stretched along the direction of channel depth, S_m and S_r were approximately treated as ovals. (d) Critical inlet flow Q_c corresponding to cells with diameters of 9 ~ 13 μm and Young's modulus of 0.5 ~ 2.5 kPa.

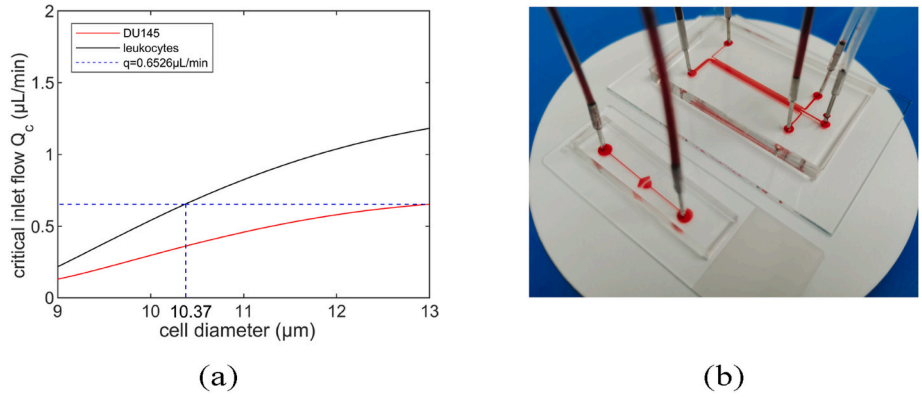

Fig. 5. (a) Critical inlet flow of DU145 cells and leukocytes. (b) The DMC two-array DLD chip and cone channel chip.

"Ethical Review Measures for Biomedical Research Involving Human Beings" (2016) of China, the "Helsinki Declaration" (2013) of WMA, and the "International Ethical Guidelines for Biomedical Research on Human Beings" (2002) of CIOMS, the experimental protocols were approved by the Institutional Ethical Committee (IEC) of the Second Hospital of Jilin University (No.2020 (182)) and the application to waive informed consent was approved.

Buffer and all volumes of the sample were injected into a CTCs sorter system (Fig. 6a) constructed by parallelizing four DMC two-array DLD chips. Small-diameter blood cells were always flowing at the chip bottom. Medium- and large-diameter cells gradually moved to the chip middle in the first array and were blocked in the chip middle by the baffle, which maintained the clean of the headspace of the second array. Large-diameter cells in the second array gradually moved towards the chip top and were separated from medium-diameter cells. Large-, medium-, and small-diameter cells flowed out from the top outlet, middle outlet, and bottom outlet, respectively (Fig. 7a ~Fig. 7e, see videos S8 ~S12). Trajectories of cells were consistent with FSI simulations (Fig. 6b, see SI and videos S4 ~S6).

The concentrations of the collected DU145 cells were calculated using a fluorescence microscope (Olympus, JPN) by Eq. (5). The CTCs sorter system was able to process a sample of 2.5 mL per minute with a recovery efficiency of 96.30 ± 2.10%, and a purity of 98.25 ± 2.48% in the top outlet. The leukocytes and DU145 cells in middle outlet were depleted of erythrocytes, platelets, and small leukocytes, which were easier to further purify using the cone channel chip. In some size-based microfluidic separation devices, these cancer cells were all lost. The DMC two-array DLD chip with only 32 periods had a simple structure, but the sorting performance was higher than most label free microfluidic sorting techniques (see SI), which was attributed to the excellent fluid regulation capability of DMC.

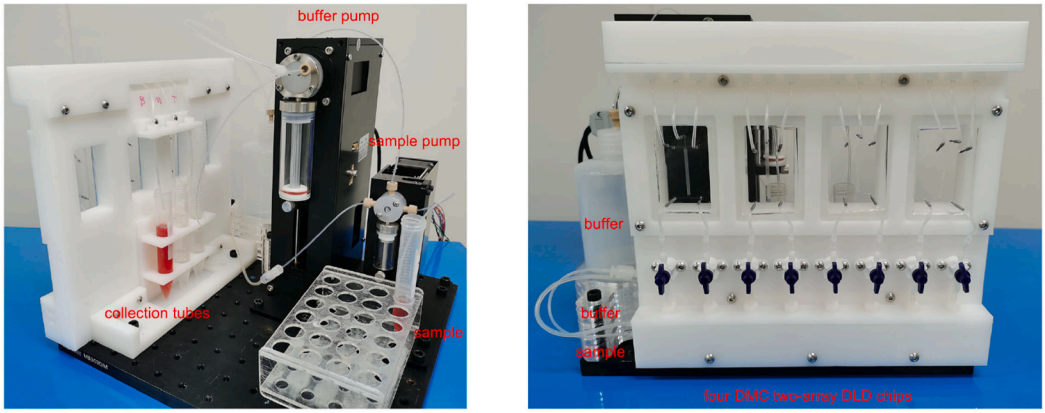

(a)

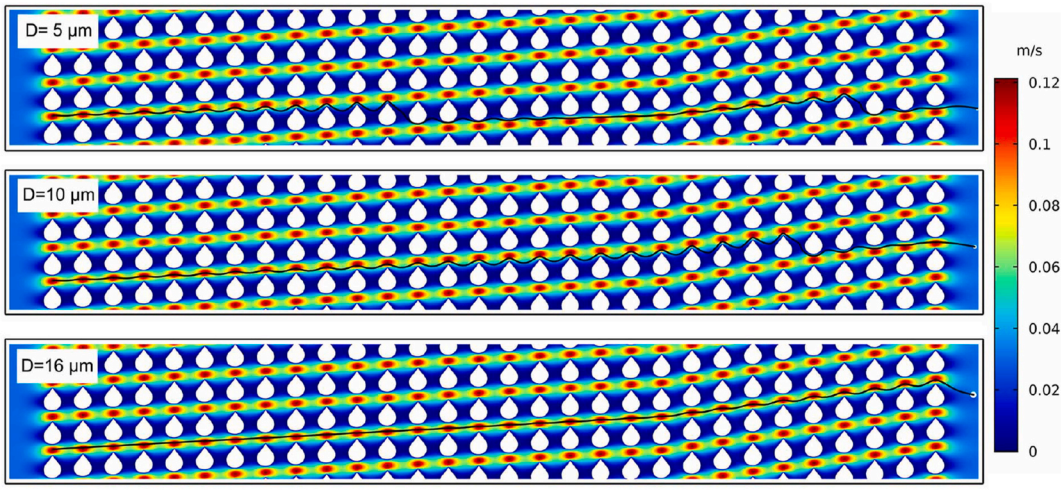

(b)

Fig. 6. (a) The CTCs sorter system. The buffer pump connects the buffer bottle and chip buffer channel. The sample pump connected buffer bottle, blood sample and chip sample channel. The three outlet tubes respectively collect large-diameter, medium-diameter and small-diameter cells. (b) The simulation of trajectories of particles within the DMC two-array DLD chip.

$$\begin{cases} \text{efficiency} = \dfrac{\text{collected cancer cells}}{\text{labeled cancer cells}} \times 100\% \\ \text{purity} = \dfrac{\text{collected cancer cells}}{\text{all collected cells}} \times 100\% \end{cases} \tag{5}$$

5.4. Separation experiment of the cone channel chip

The concentration of the cell mixture from the middle outlet of the DMC two-array DLD chip was manually adjusted and injected into the cone channel chip. When the inlet flow rate was 25 μL/min, slightly larger sized cells were trapped at the end of the channel (Fig. 8a). Increasing the flow rate to 68 μL/min (the corresponding single cone channel flow rate was 0.66 μL/min) according to Fig. 5a, slightly larger sized DU145 cells passed through the cone channel (Fig. 8b). The cone channel entrapped stiffer leukocytes and freed softer DU145 cells, as shown in Fig. 9. Therefore, it was feasible to separate cells that are close in size but different in stiffness by controlling the flow rate to adjust the hydrodynamic force. A few of DU145 cells were entrapped at the end of the cone channel, probably because of friction and adhesion.

After a period of cone channel chip run, random entry of cells into some channels allowed acceleration of flow rates within others. Therefore, when cone channels were used in parallel, the actual optimum flow rate was less than the theoretical value and closely related to the cell concentration of the sample as well as the number of parallel channels. For the medium-diameter sample with a concentration of $1 \times 10^3/mL$ and cone channel array with a parallel number of 104, the chip was run for about 80*s* at a flow rate of 35 μL/min, which allowed a near optimal flow rate, and the purity of DU145 cells increased from 9.3% to 16.67% about 1.8-fold. The inability to control a single cell resulted in multiple cells entering the same channel hindering isolation, so only 75% of DU145 cells were collected. For example, within the channel indicated by the black arrow (Fig. 9), subsequent smaller-sized cell cannot pass through the channel because the previous cell was trapped.

5.5. ROS measurement

Reactive oxygen species (ROS) play a mediating role in cell life, stress, and death, and different concentrations of ROS lead to different fates of cells (Dröge, 2002; Verbon et al., 2012). The detection results of intracellular ROS levels using a commercial kit (Biosharp, CHN) showed that the DMC two-array DLD chip could maintain cell activity; The cone channel chip could maintain the activity of slightly smaller-sized cells, but there might be a slight effect on slightly larger-sized cells. See SI for details.

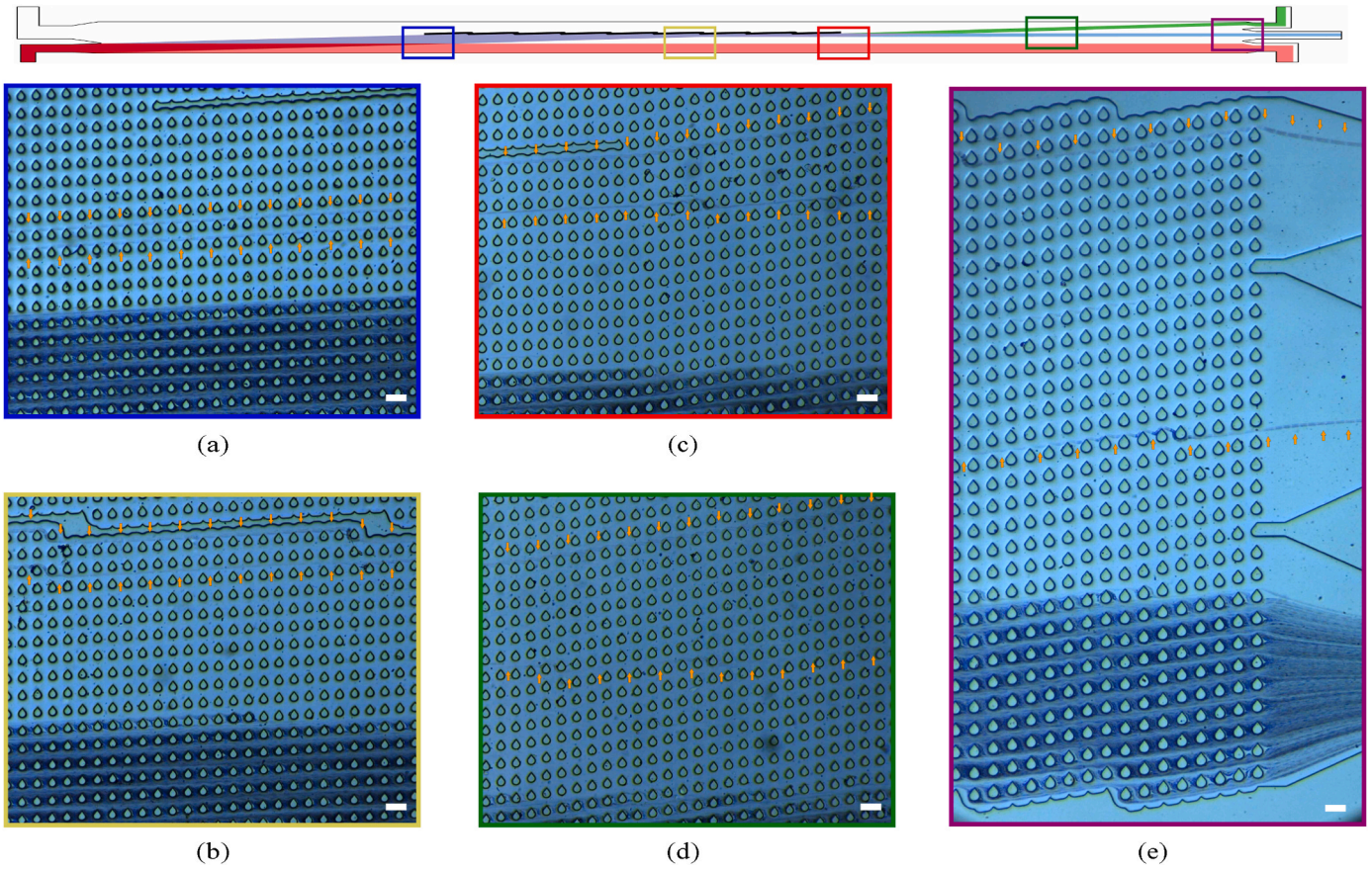

Fig. 7. Camera (FASTCAM UX100, JPN) images were superimposed over successive times to show cell trajectories. Scale bar was 100 μm. See videos S8 ~S12. (a) Medium - and large-diameter cells began to separate from small-diameter cells. (b) Large - and medium-diameter cells completed separation from small-diameter cells and were confined to the middle of the chip by baffles. (c) Medium - and large-diameter cells began to separate from each other. (d) Medium - and large-diameter cells completed separation. (e) Large-, medium-, and small-diameter cells flowed out from the top outlet, middle outlet, and bottom outlet, respectively.

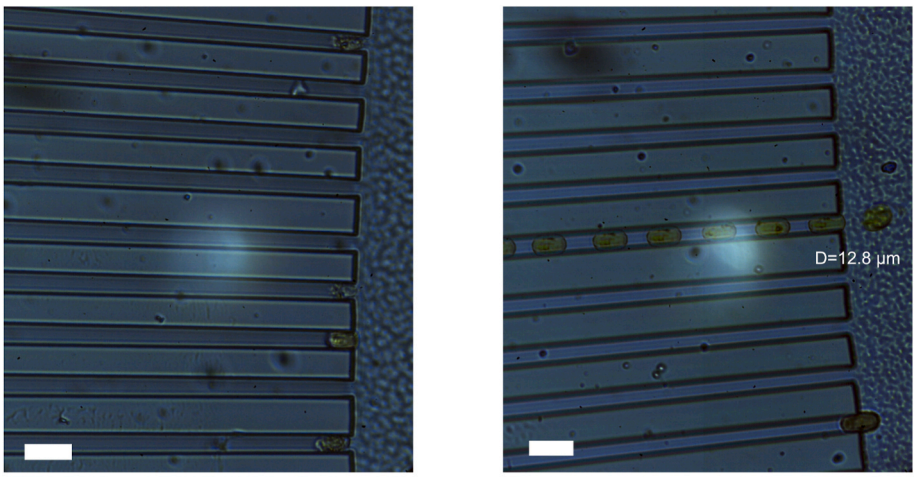

Fig. 8. (a) Cells of slightly larger size were captured with a flow rate of 25 μL/min. See video S13. (b) DU145 cell passed through the channel with a flow rate of 68 μL/min. Images were superimposed over successive time with a scale bar of 20 μm. See video S14.

5.6. Raman analysis of leukocytes and CTCs

The collected cancer cells were dropped onto glass slides. The integration time of the Raman microspectrograph (Fig. 10a) built in our lab was 10*s* and repeated 3 times at a laser intensity of 50*mw*. The glass Raman signal and background fluorescence were removed using the LM-SG algorithms (Chi et al., 2019; Han et al., 2020). Based on a Raman spectral classification model (Fig. 10b) with ten fold cross validation accuracy higher than 98.5% built using 64 DU145 cells and 80 healthy leukocytes, DU145 cells and leukocytes were successfully distinguished using the PCA-LDA algorithm (Dochow et al., 2011).

1 mL of whole blood from a cancer patient diagnosed at the Second

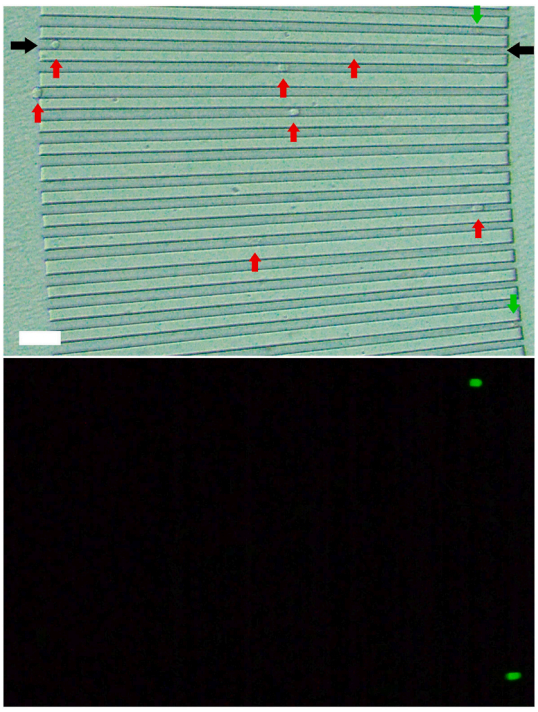

Fig. 9. Leukocytes of slightly larger size (red arrows) were trapped within the channel, whereas only a few DU145 cells (green arrows) were trapped in the back of the channel. The inlet flow was 35 μL/min and scale bar was 50 μm.

Hospital of Jilin University was diluted 20-fold and then completely sorted using the CTCs sorter system, and the cells from the top outlet were collected and concentrated. From the two samples, 5 and 18 cancer cells were identified, respectively, according to the Raman spectral classification model, indicating that the system is applicable to real clinical samples.

6. Conclusions

In this study, we presented a multistage microfluidic CTCs sorting method, first sorting CTCs using a size-based two-array DLD chip, then purifying CTCs mixed by leukocytes using a stiffness-based cone channel chip, and finally identifying cell types using Raman techniques. The entire sorting and analysis process was label free, highly pure, high-throughput and efficient. This is currently the only reported hybrid whole microfluidic label free CTCs sorting analysis method that enables complete CTCs sorting and identification. This work provides a new perspective for using multiple physical properties to classify CTCs, which can improve specificity and reduce the impact of heterogeneity. This system enables sorting analysis of cancer cells from clinical samples that only require dilution and has the potential to be developed into a one-stop label-free high-performance sorting analysis system for CTCs.

The DMC was obtained by optimized design rather than the empirical design, and its fluid regulation ability was superior to that of conventional microcolumn topography, greatly improving the sorting performance of DLD. The parameterized design process of DMC offered substantial cost savings, and this optimization method is also applicable to other microfluidic device designs, such as optimizing the micromixer structure to achieve quantitative mixing of multiple fluids. The tip of DMC of PDMS material is easily distorted, but a hard mold suitable for batch production can enhance hardness. Relying on the excellent fluid regulation capability of DMC, the sorting performance of size-based DMC two-array DLD chip surpassed most label free technologies. Since the current structural design of the DMC two-array DLD chip was very simple, we believed that the potential of DMC can be further mined by optimizing the overall structure.

The cone channel chip was used to purify CTCs mixed dimensionally by leukocytes to achieve complete sorting. These CTCs are difficult to isolate in several other size-based label free microfluidic devices. As a new common device with simple structure, the cone channel chip separates cells based on the most primitive physical characteristics with only one compression and without the external force field, and enables serve as the back end of many size-based microfluidic technologies to purify cancer cells. It is essentially a microfiltration technique with a restricted optimal inlet flow, so the chip array needs to be set to separate continuously flowing samples, and the sample concentration needs to be adjusted to reduce clogging. Based on the above reasons, and the high flow resistance of the cone channel structure, we believed that the cone channel chip array is more suitable for separation application rather than one-piece application when interfaced with other continuous flow microfluidic technologies. We estimated that the stiffness properties of

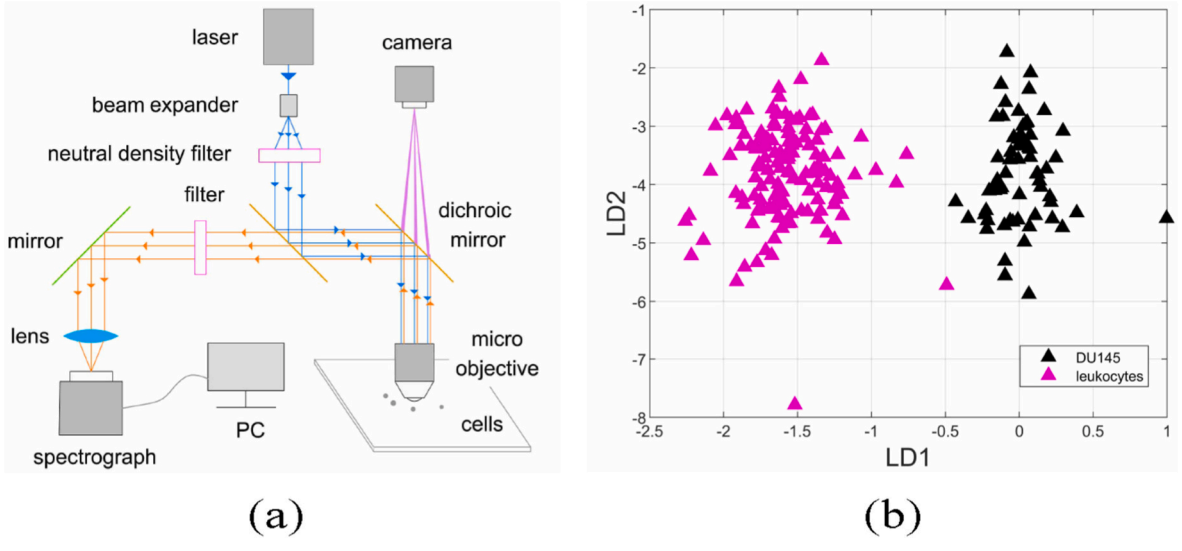

Fig. 10. (a) Schematic diagram of Raman microspectrograph. The system used a 532 nm excitation light source of 200*mw*. The laser was focused through a 50 × microscope objective (Olympus, JPN) into a 2 μm spot. An Andor CCD camera was used to detect the Raman signal after dispersion. The Raman spectra of 400 ~ 1800 cm^{-1} spectral range were recorded, and the resolution was approximately 2 cm^{-1}. A neutral density filter (THORLABS NE05B) was used to attenuate the laser intensity to 50*mw*. (b) Cluster analysis of DU145 cells and leukocytes after PCA-LDA algorithm calculation.

CTCs and leukocytes of other size ranges are consistent, so they can still be distinguished by the cone channels. Because cell relaxation occurs upon prolonged contact with the channel, the viscoelastic (Wang et al., 2021), adhesive, and frictional properties of the cells need to be further discussed to understand the mechanisms of cell movement and deformation within the cone channel.

Compatible with microfluidic label free CTCs sorting methods, Raman spectroscopy offers the advantages of being label free, low destructive, highly sensitive and strongly specific (Chai et al., 2022) and can non-invasively probe metabolites within a single living cell (Du et al., 2020). Combining microfluidic sorting technology with Raman analysis is of great significance in constructing a one-stop CTCs sorting and analysis system and advancing the laboratory detection and clinical application of CTCs.

Acknowledgements

This work was supported by the National Natural Science Foundation of China (U21A20395 and 61727813). The author thanks Changchun University of Science and Technology for their assistance in AFM.

CRediT authorship contribution statement

Gaolin Li: Writing – original draft, Validation, Formal analysis, Visualization, Conceptualization, Data curation. **Yuan Ji:** Methodology. **Yihui Wu:** Methodology, Writing – review & editing, Funding acquisition, Resources, Supervision, Project administration. **Yongshun Liu:** Resources. **Huan Li:** Methodology, Writing – review & editing. **Yimeng Wang:** Formal analysis. **Mingbo Chi:** Formal analysis, Methodology. **Hongyan Sun:** Resources. **Hongquan Zhu:** Resources, Methodology.

Declaration of competing interest

The authors declare that they have no known competing financial interests or personal relationships that could have appeared to influence the work reported in this paper.

Data availability

Data will be made available on request.

Appendix A. Supplementary data

Supplementary data to this article can be found online at https://doi.org/10.1016/j.bios.2023.115451.

References

Al-Fandi, M., Al-Rousan, M., Jaradat, M.A., Al-Ebbini, L., 2011. New design for the separation of microorganisms using microfluidic deterministic lateral displacement. Robot. Comput. Integrated Manuf. 27, 237–244. https://doi.org/10.1016/j.rcim.2010.06.003.

Allard, W.J., Matera, J., Miller, M.C., Repollet, M., Connelly, M.C., Rao, C., Tibbe, A.G.J., Uhr, J.W., Terstappen, L.W.M.M., 2004. Tumor cells circulate in the peripheral blood of all major carcinomas but not in healthy subjects or patients with nonmalignant diseases. Clin. Cancer Res. 10, 6897–6904. https://doi.org/10.1158/1078-0432.CCR-04-0378.

Au, S.H., Edd, J., Stoddard, A.E., Wong, K.H., Fachin, F., Maheswaran, S., Haber, D.A., Stott, S.L., Kapur, R., Toner, M., 2017. Microfluidic isolation of circulating tumor cell clusters by size and asymmetry. Sci. Rep. 7, 1–10. https://doi.org/10.1038/s41598-017-01150-3.

Beech, J.P., Ho, B.D., Garriss, G., Oliveira, V., Henriques-Normark, B., Tegenfeldt, J.O., 2018. Separation of pathogenic bacteria by chain length. Anal. Chim. Acta 1000, 223–231. https://doi.org/10.1016/j.aca.2017.11.050.

Beech, J.P., Jönsson, P., Tegenfeldt, J.O., 2009. Tipping the balance of deterministic lateral displacement devices using dielectrophoresis. Lab Chip 9, 2698–2706. https://doi.org/10.1039/B823275J.

Celik, E., Rongione, N., Bahamonde, A., Ao, Z., Datar, R., 2015. Isolation of circulating tumor cells using stiffness-based filtration platform. In: ASME International Mechanical Engineering Congress and Exposition. ASME, V003T03A079. https://doi.org/10.1115/IMECE2015-53241.

Chai, S., Sun, X., Fu, C., Xu, Q., Ren, Z., Xie, L., Ge, J., Sang, M., 2022. Identification and characterization of the inhibitory effect of art on colorectal cancer cells using Raman spectroscopy. J. Raman Spectrosc. 53, 191–201. https://doi.org/10.1002/jrs.6292.

Chen, C.L., Mahalingam, D., Osmulski, P., Jadhav, R.R., Wang, C.M., Leach, R.J., Chang, T.C., Weitman, S.D., Kumar, A.P., Sun, L., Gaczynska, M.E., Thompson, I.M., Huang, T.H.M., 2013. Single-cell analysis of circulating tumor cells identifies cumulative expression patterns of emt-related genes in metastatic prostate cancer. Prostate 73, 813–826. https://doi.org/10.1002/pros.22625.

Chen, X., Feng, Q., Zhang, Y., 2022. Insights into a deterministic lateral displacement sorting chip with new cross-section micropillars. Chaos, Solit. Fractals 156, 111884. https://doi.org/10.1016/j.chaos.2022.111884.

Chi, M., Han, X., Xu, Y., Wang, Y., Shu, F., Zhou, W., Wu, Y., 2019. An improved background-correction algorithm for Raman spectroscopy based on the wavelet transform. Appl. Spectrosc. 73, 78–87. https://doi.org/10.1177/0003702818805116.

Cormack, D.H., 2001. Essential Histology. Lippincott Williams & Wilkins.

Cross, S.E., Jin, Y.S., Rao, J., Gimzewski, J.K., 2007. Nanomechanical analysis of cells from cancer patients. Nat. Nanotechnol. 2, 780–783. https://doi.org/10.1038/nnano.2007.388.

Davis, J.A., 2008. Microfluidic Separation of Blood Components through Deterministic Lateral Displacement. Princeton University.

Dochow, S., Krafft, C., Neugebauer, U., Bocklitz, T., Henkel, T., Mayer, G., Albert, J., Popp, J., 2011. Tumour cell identification by means of Raman spectroscopy in combination with optical traps and microfluidic environments. Lab Chip 11, 1484–1490. https://doi.org/10.1039/C0LC00612B.

Dröge, W., 2002. Free radicals in the physiological control of cell function. Physiol. Rev. https://doi.org/10.1152/physrev.00018.2001.

Du, J., Su, Y., Qian, C., Yuan, D., Miao, K., Lee, D., Ng, A.H., Wijker, R.S., Ribas, A., Levine, R.D., et al., 2020. Raman-guided subcellular pharmaco-metabolomics for metastatic melanoma cells. Nat. Commun. 11, 4830. https://doi.org/10.1038/s41467-020-18376-x.

Han, X., Wu, Y., Chi, M., Gao, S., Wang, Q., 2020. Single-cell Raman spectrum extraction from clinic biosamples. J. Raman Spectrosc. 51, 2255–2264. https://doi.org/10.1002/jrs.5984.

Henry, E., Holm, S.H., Zhang, Z., Beech, J.P., Tegenfeldt, J.O., Fedosov, D.A., Gompper, G., 2016. Sorting cells by their dynamical properties. Sci. Rep. 6, 1–11. https://doi.org/10.1038/srep34375.

Hochstetter, A., Vernekar, R., Austin, R.H., Becker, H., Beech, J.P., Fedosov, D.A., Gompper, G., Kim, S.C., Smith, J.T., Stolovitzky, G., Tegenfeldt, J.O., Wunsch, B.H., Zeming, K.K., Krüger, T., Inglis, D.W., 2020. Deterministic lateral displacement: challenges and perspectives. ACS Nano 14, 10784–10795. https://doi.org/10.1021/acsnano.0c05186.

Hou, S., Zhao, H., Zhao, L., Shen, Q., Wei, K.S., Suh, D.Y., Nakao, A., Garcia, M.A., Song, M., Lee, T., et al., 2013. Capture and stimulated release of circulating tumor cells on polymer-grafted silicon nanostructures. Adv. Mater. 25, 1547–1551. https://doi.org/10.1002/adma.201203185.

Huang, L.R., Cox, E.C., Austin, R.H., Sturm, J.C., 2004. Continuous particle separation through deterministic lateral displacement. Science 304, 987–990. https://doi.org/10.1126/science.1094567.

Hyun, K.A., Kwon, K., Han, H., Kim, S.I., Jung, H.I., 2013. Microfluidic flow fractionation device for label-free isolation of circulating tumor cells (ctcs) from breast cancer patients. Biosens. Bioelectron. 40, 206–212. https://doi.org/10.1016/j.bios.2012.07.021.

Inglis, D.W., Davis, J.A., Austin, R.H., Sturm, J.C., 2006. Critical particle size for fractionation by deterministic lateral displacement. Lab Chip 6, 655–658. https://doi.org/10.1039/B515371A.

Islam, M., Brink, H., Blanche, S., DiPrete, C., Bongiorno, 2017. Microfluidic sorting of cells by viability based on differences in cell stiffness. Sci. Rep. 7, 1–12. https://doi.org/10.1038/s41598-017-01807-z.

Islam, M., Raj, A., McFarland, B., Brink, H.M., Ciciliano, J., Fay, M., Myers, D.R., Flowers, C., Waller, E.K., Lam, W., Alexeev, A., Sulchek, T., 2020. Stiffness based enrichment of leukemia cells using microfluidics. APL Bioeng 4, 036101. https://doi.org/10.1063/1.5143436.

Jiang, X., Wong, K.H.K., Khankhel, A.H., Zeinali, M., Reategui, E., Phillips, M.J., Luo, X., Aceto, N., Fachin, F., Hoang, A.N., Kim, W., Jensen, A.E., Sequist, L.V., Maheswaran, S., Haber, D.A., Stott, S.L., Toner, M., 2017. Microfluidic isolation of platelet-covered circulating tumor cells. Lab Chip 17, 3498–3503. https://doi.org/10.1039/C7LC00654C.

Karabacak, N.M., Spuhler, P.S., Fachin, F., Lim, E.J., Pai, V., Ozkumur, E., Martel, J.M., Kojic, N., Smith, K., Chen, P.i., et al., 2014. Microfluidic, marker-free isolation of circulating tumor cells from blood samples. Nat. Protoc. 9, 694–710. https://doi.org/10.1038/nprot.2014.044.

Kuznetsova, T.G., Starodubtseva, M.N., Yegorenkov, N.I., Chizhik, S.A., Zhdanov, R.I., 2007. Atomic force microscopy probing of cell elasticity. Micron 38, 824–833. https://doi.org/10.1016/j.micron.2007.06.011.

Loiko, V.A., Ruban, G.I., Gritsai, O.A., Berdnik, V.V., Goncharova, N.V., 2007. Mononuclear cells morphology for cells discrimination by the angular structure of scattered light. In: Tenth Conference on Electromagnetic and Light Scattering. Begel House Inc., pp. 105–108. https://doi.org/10.1615/ICHMT.2007.ConfElectromagLigScat.290

Loutherback, K., Chou, K.S., Newman, J., Puchalla, J., Austin, R.H., Sturm, J.C., 2010. Improved performance of deterministic lateral displacement arrays with triangular posts. Microfluid. Nanofluidics 9, 1143–1149. https://doi.org/10.1007/s10404-010-0635-y.

Low, W.S., Wan Abas, W.A.B., 2015. Benchtop technologies for circulating tumor cells separation based on biophysical properties. BioMed Res. Int. 2015, 1–22. https://doi.org/10.1155/2015/239362.

Marrinucci, D., Bethel, K., Lazar, D., Fisher, J., Huynh, E., Clark, P., Bruce, R., Nieva, J., Kuhn, P., 2010. Cytomorphology of circulating colorectal tumor cells: a small case series. J ONCOL 2010. https://doi.org/10.1155/2010/861341.

Pariset, E., Parent, C., Fouillet, Y., François, B., Verplanck, N., Revol-Cavalier, F., Thuaire, A., Agache, V., 2018. Separation of biological particles in a modular platform of cascaded deterministic lateral displacement modules. Sci. Rep. 8, 1–10. https://doi.org/10.1038/s41598-018-34958-8.

Qian, W., Zhang, Y., Chen, W., 2015. Capturing cancer: emerging microfluidic technologies for the capture and characterization of circulating tumor cells. Small 11, 3850–3872. https://doi.org/10.1002/smll.201403658.

Roca-Cusachs, P., Almendros, I., Sunyer, R., Gavara, N., Farré, R., Navajas, D., 2006. Rheology of passive and adhesion-activated neutrophils probed by atomic force microscopy. Biophys. J. 91, 3508–3518. https://doi.org/10.1529/biophysj.106.088831.

Seifter, J., Sloane, D., Ratner, A., 2005. Concepts in Medical Physiology. Lippincott Williams & Wilkins.

Thompson, A.M., Paguirigan, A.L., Kreutz, J.E., Radich, J.P., Chiu, D.T., 2014. Microfluidics for single-cell genetic analysis. Lab Chip 14, 3135–3142. https://doi.org/10.1039/C4LC00175C.

Vaidyanathan, R., Soon, R.H., Zhang, P., Jiang, K., Lim, C.T., 2019. Cancer diagnosis: from tumor to liquid biopsy and beyond. Lab Chip 19, 11–34. https://doi.org/10.1039/C8LC00684A.

Verbon, E.H., Post, J.A., Boonstra, J., 2012. The influence of reactive oxygen species on cell cycle progression in mammalian cells. Gene 511, 1–6. https://doi.org/10.1016/j.gene.2012.08.038.

Wang, G., Mao, W., Byler, R., Patel, K., Henegar, C., Alexeev, A., Sulchek, T., 2013. Stiffness dependent separation of cells in a microfluidic device. PLoS One 8, e75901. https://doi.org/10.1371/journal.pone.0075901.

Wang, J., Tang, X., Wang, Z., Li, J., Ma, S., 2021. Extracellular scaffold design for ultra-soft microtissue engineering. LAM 2, 173–185. https://doi.org/10.37188/lam.2021.011.

Wills, Q.F., Mead, A.J., 2015. Application of single-cell genomics in cancer: promise and challenges. Hum. Mol. Genet. 24, R74–R84. https://doi.org/10.1093/hmg/ddv235.

Xu, W., Mezencev, R., Kim, B., Wang, L., McDonald, J., Sulchek, T., 2012. Cell stiffness is a biomarker of the metastatic potential of ovarian cancer cells. PLoS One e46609doi. https://doi.org/10.1371/journal.pone.0046609.

Xue, S., Xu, Q., Xu, Z., Zhang, X., Zhang, H., Zhang, X., He, F., Chen, Y., Xue, Y., Hao, P., 2023. Manipulation of particle/cell based on compressibility in a divergent microchannel by surface acoustic wave. Anal. Chem. 95, 4282–4290. https://doi.org/10.1021/acs.analchem.2c03841.

Yeo, T., Tan, S.J., Lim, C.L., Lau, D.P., Chua, Y.W., Krisna, S.S., Iyer, G., Tan, G.S., Lim, T. K., Tan, D.S., Lim, W.T., Lim, C.T., 2016. Microfluidic enrichment for the single cell analysis of circulating tumor cells. Sci. Rep. 6, 22076 https://doi.org/10.1038/srep22076.

Zeming, K.K., Ranjan, S., Zhang, Y., 2013. Rotational separation of non-spherical bioparticles using i-shaped pillar arrays in a microfluidic device. Nat. Commun. 4, 1–8. https://doi.org/10.1038/ncomms2653.

Zeming, K.K., Salafi, T., Chen, C.H., Zhang, Y., 2016. Asymmetrical deterministic lateral displacement gaps for dual functions of enhanced separation and throughput of red blood cells. Sci. Rep. 6, 1–10. https://doi.org/10.1038/srep22934.

Zhang, Z., Henry, E., Gompper, G., Fedosov, D.A., 2015. Behavior of rigid and deformable particles in deterministic lateral displacement devices with different post shapes. J. Chem. Phys. 143, 243145 https://doi.org/10.1063/1.4937171.

Zhou, Y., Ma, Z., Ai, Y., 2019. Hybrid microfluidic sorting of rare cells based on high throughput inertial focusing and high accuracy acoustic manipulation. RSC Adv. 9, 31186–31195. https://doi.org/10.1039/C9RA01792E.